Hydrophobic Modulation of Heme Properties in Heme Protein Maquettes †

ARTICLE *in* BIOCHEMISTRY · OCTOBER 2001

Impact Factor: 3.02 · DOI: 10.1021/bi002806h · Source: PubMed

6 AUTHORS, INCLUDING:

Brian R Gibney
City University of New York - Brooklyn College
78 PUBLICATIONS **2,927** CITATIONS
SEE PROFILE

Ernesto J Fuentes
University of Iowa
27 PUBLICATIONS **870** CITATIONS
SEE PROFILE

Andrew Joshua Wand
University of Pennsylvania
193 PUBLICATIONS **8,748** CITATIONS
SEE PROFILE

Hydrophobic Modulation of Heme Properties in Heme Protein Maquettes†

Brian R. Gibney,‡ Steve S. Huang, Jack J. Skalicky,§ Ernesto J. Fuentes, A. Joshua Wand, and P. Leslie Dutton*

The Johnson Research Foundation, Department of Biochemistry and Biophysics, School of Medicine, University of Pennsylvania, Philadelphia, Pennsylvania 19104

Received December 11, 2000; Revised Manuscript Received April 9, 2001

ABSTRACT: We have investigated the properties of the two hemes bound to histidine in the H10 positions of the uniquely structured apo form of the heme binding four-helix bundle protein maquette [H10H24-L6I,L13F]$_2$, here called [$I_6F_{13}H_{24}$]$_2$ for the amino acids at positions 6 (I), 13 (F) and 24 (H), respectively. The primary structure of each α-helix, α-SH, in [$I_6F_{13}H_{24}$]$_2$ is Ac-CGGGEI^{6}WKL·H^{10}EEF^{13}LKK·FEELLKL·H^{24}EERLKK·L-CONH$_2$. In our nomenclature, [$I_6F_{13}H_{24}$] represents the disulfide-bridged di-α-helical homodimer of this sequence, i.e., (α-SS-α), and [$I_6F_{13}H_{24}$]$_2$ represents the dimeric four helix bundle composed of two di-α-helical subunits, i.e., (α-SS-α)$_2$. We replaced the histidines at positions H24 in [$I_6F_{13}H_{24}$]$_2$ with hydrophobic amino acids incompetent for heme ligation. These maquette variants, [$I_6F_{13}I_{24}$]$_2$, [$I_6F_{13}A_{24}$]$_2$, and [$I_6F_{13}F_{24}$]$_2$, are distinguished from the tetraheme binding parent peptide, [$I_6F_{13}H_{24}$]$_2$, by a reduction in the heme:four-helix bundle stoichiometry from 4:1 to 2:1. Iterative redesign has identified phenylalanine as the optimal amino acid replacement for H24 in the context of apo state conformational specificity. Furthermore, the novel second generation diheme [$I_6F_{13}F_{24}$]$_2$ maquette was related to the first generation diheme [H10A24]$_2$ prototype, [$L_6L_{13}A_{24}$]$_2$ in the present nomenclature, via a sequential path in sequence space to evaluate the effects of conservative hydrophobic amino acid changes on heme properties. Each of the disulfide-linked dipeptides studied was highly helical (>77% as determined from circular dichroism spectroscopy), self-associates in solution to form a dimer (as determined by size exclusion chromatography), is thermodynamically stable ($-\Delta G^{H_2O}$ >18 kcal/mol), and possesses conformational specificity that NMR data indicate can vary from multistructured to single structured. Each peptide binds one heme with a dissociation constant, K_{d1} value, tighter than 65 nM forming a series of monoheme maquettes. Addition of a second equivalent of heme results in heme binding with a K_{d2} in the range of 35−800 nM forming the diheme maquette state. Single conservative amino acid changes between peptide sequences are responsible for up to 10-fold changes in K_d values. The equilibrium reduction midpoint potential ($E_{m7.5}$) determined in the monoheme state ranges from −156 to −210 mV vs SHE and in the diheme state ranges from −144 to −288 mV. An observed heme−heme electrostatic interaction (>70 mV) in the diheme state indicates a syn global topology of the di-α-helical monomers. The heme affinity and electrochemistry of the three H24 variants studied identify the tight binding sites (K_{d1} and K_{d2} values <200 nM) having the lower reduction midpoint potentials ($E_{m7.5}$ values of −155 and −260 mV) with the H10 bound hemes in the parent tetraheme state of [H10H24-L6I,L13F]$_2$, here called [$I_6F_{13}H_{24}$]$_2$. The results of this study illustrate that conservative hydrophobic amino acid changes near the heme binding site can modulate the E_m by up to ±50 mV and the K_d by an order of magnitude. Furthermore, the effects of multiple single amino acid changes on E_m and K_d do not appear to be additive.

Maquettes (*1*), simplified functional versions of complex native enzymes, provide a biochemical framework within which to constructively test hypotheses about enzyme structure−function relationships. On the basis of a generic (α-SS-α)$_2$ architecture, the tetra-α-helical bundle maquettes provide a highly stable and robust protein assembly that is amenable to primary amino acid sequence alterations without large-scale structural perturbation (*2*, *3*). Using dimeric maquette scaffolds, we have incorporated a variety of biochemically derived prosthetic groups and cofactors including hemes and other metalloporphyrins (*1*, *4*), free base porphyrin dimers (*5*), nitroxide spin labels representing amino acid radicals (*6*), iron−sulfur clusters (*7*), and flavins (*8*) for study within a physiologically relevant environment. Additionally, combinations of cofactors such as hemes B and hemes A (*9*), hemes and iron−sulfur clusters (*7*), and hemes and flavins (*8*) yield constructs suitable for systematic investigations of the interaction between cofactors with their synthetic peptide hosts.

Within the (α-SS-α)$_2$ scaffold, we are investigating fundamental biochemical issues of metalloprotein assembly, structure, and function (*10*, *11*). The tetraheme containing

† This work was supported by National Institutes of Health grants to P.L.D. (GM 48130) and A.J.W. (GM 35940) and partly by the MRSEC-IRG Program from the National Science Foundation (DMR00-79909). Mass spectroscopic analyses were performed by the Protein Chemistry Laboratory of the University of Pennsylvania.

* Corresponding author. Phone: (215) 898-5668. Fax: (215) 573-2235. E-mail: dutton@mail.med.upenn.edu.

‡ Current address: Department of Chemistry, Columbia University, New York, NY 10027.

§ Current address: Department of Chemistry, State University of New York, Buffalo, NY 14260-3000.

10.1021/bi002806h CCC: $20.00
Published on Web 08/11/2001

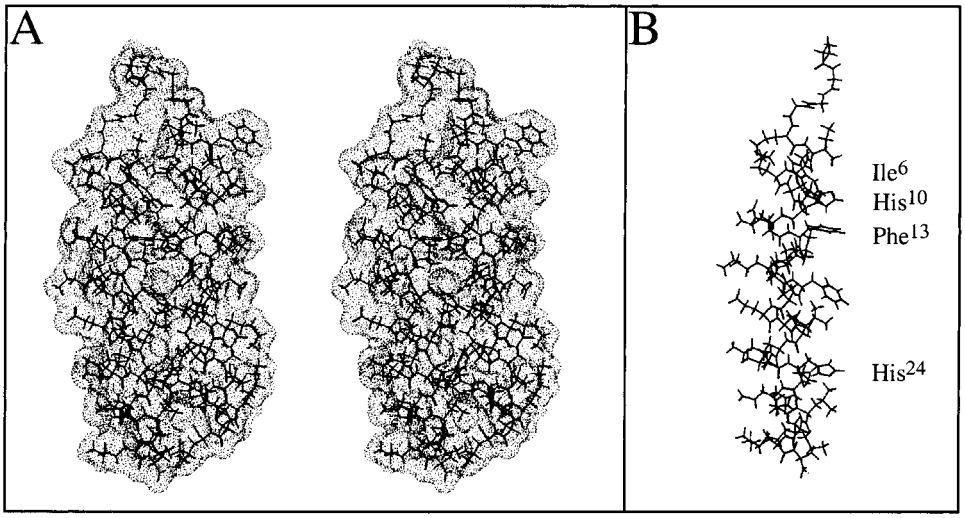

FIGURE 1: Representation of the apo-$[I_6F_{13}H_{24}]_2$ monomer NMR solution structure. The surface representation, panel A, illustrates the lack of a classic heme binding pocket in the vicinity of either the H10 or H24 binding sites. The sites of modification are labeled on the single helix in panel B, which demonstrates orientation of the peptide with the H10 site on top.

tetra-α-helical protein, $[H10H24]_2$ (*1*) ($[L_6L_{13}H_{24}]_2$ in the present nomenclature), was designed to model the key structural features of the cytochrome bc_1 respiratory complex III (ubiquinol:cytochrome *c* oxidoreductase, EC 1.10.2.2) (*12*−*14*) and has served as the prototype heme maquette in our hierarchical approach (*15*) to heme protein design. Using this scaffold, we have investigated protein−protein assembly by designing conformationally specific proteins (*2*, *3*, *16*) that provide an experimental view of sequence space, the landscape of all protein sequences. Additionally, we have used maquettes to study protein−cofactor interactions that define the basic engineering specifications requisite for heme and iron−sulfur incorporation and the breadth of their tolerances (*11*, *17*) and heme−heme electrostatic communication (cofactor−cofactor interactions) which provides a method to define the relative global topology of the two di-α-helical protein subunits of diheme $(\alpha\text{-SS-}\alpha)_2$ (*18*). This versatile model system has also allowed investigations of intercofactor electron transfer (*8*) and coupled electron/proton transfer (proton uptake/release during heme reduction/oxidation) (*19*), processes fundamental to bioenergetics and ubiquitous within biochemistry.

Herein, we trace a continuous path in sequence space from the second generation prototype tetraheme protein maquette $[I_6F_{13}H_{24}]_2$ (named for its amino acids at positions 6, 13, and 24 and shown in Figure 1), which is conformationally specific in the apo state and whose structure has recently been determined via solution NMR[1] methodologies (*20*, *21*), to the first generation prototype diheme $[L_6L_{13}A_{24}]_2$ maquette (*1*). Our purpose was twofold: first, to define the properties of the hemes bound to the H10 sites in $[I_6F_{13}H_{24}]_2$; second, to investigate the role of sequential hydrophobic amino acid changes in heme affinity and electrochemistry and map these in functional sequence space. For system simplification, we replaced the four histidine ligands at helix positions 24 in $[I_6F_{13}H_{24}]_2$, called $[IFL]_2$ in ref 3, with the hydrophobic amino acids alanine, isoleucine, and phenylalanine, chosen for their range of steric and conformational properties on the α-helical structure and their incompetence for iron ligation. The resulting three peptides, designated $[I_6F_{13}A_{24}]_2$, $[I_6F_{13}I_{24}]_2$, and $[I_6F_{13}F_{24}]_2$, bind only two hemes per four-helix bundle, as designed, confirming the obligate role of histidine in iron ligation. Since $[I_6F_{13}F_{24}]_2$ is only three amino acids different than the well-characterized prototype $[L_6L_{13}A_{24}]_2$, a series of three modified versions of $[L_6L_{13}A_{24}]_2$ were made to link it to $[I_6F_{13}F_{24}]_2$ by a path in sequence space. This series of peptides can be also used to evaluate the feasibility of rational evolution of heme properties in designed proteins. The data presented clearly demonstrate that the amino acid changes to $[L_6L_{13}H_{24}]_2$ responsible for a gain in conformational specificity transfer to the related $[L_6L_{13}A_{24}]_2$ scaffold. Direct evidence for oxidized heme affinity is presented for each peptide studied. The electrochemistry of each peptide in two distinct states (one and two hemes bound) demonstrates a low dielectric hydrophobic core which supports heme−heme electrostatic interactions and, furthermore, defines the global topology of the diheme proteins. Finally, a correlation of apoprotein conformational specificity and heme reduction potentials of the single heme bound states demonstrates that hydrophobic packing modulates heme redox activity.

MATERIALS AND METHODS

Hemin, trifluoroacetic acid, diethyl ether, acetic anhydride, piperidine, and pyridine were obtained from the Aldrich Chemical Co. (Milwaukee, WI). Ethanedithiol and 1-hydroxybenzotriazole (HOBt) were purchased from Fluka (Ronkonkoma, NY). The NovaSyn PR-500 resin was purchased from Calbiochem-Novabiochem (La Jolla, CA). Natural Fmoc-protected amino acids were acquired as pentafluorophenyl esters from PerSeptive Biosystems(Framingham, MA) with the exception of Fmoc-L-Arg(Pmc)-OPfp,

[1] Abbreviations: Fmoc, 9-fluorenylmethoxycarbonyl; ^{t}Bu, *tert*-butyl; Pmc, 2,2,5,7,8-pentamethylchroman-6-sulfonyl; OPfp, pentafluorophenyl ester; CD, circular dichroism; NMR, nuclear magnetic resonance; ^{13}C HSQC, carbon-13 heteronuclear single-quantum coherence; NOE, nuclear Overhauser effect; SHE, standard hydrogen electrode; $E_{m7.5}$, equilibrium midpoint reduction potential at pH 7.5; Gdn·HCl, guanidine hydrochloride; HPLC, high-performance liquid chromatography; ΔG_{unf}, difference in Gibbs free energy between denatured and folded protein in the presence of dentaturant; ΔG^{H_2O}, difference in Gibbs free energy between denatured and folded protein in water; DMF, *N*,*N*-dimethylformamide; TFA, trifluoroacetic acid; DMSO, dimethyl sulfoxide.

which was purchased from Bachem (King of Prussia, PA). Guanidine hydrochloride (8 M) was used as received from Pierce (Rockford, IL). All other chemicals and solvents were of reagent grade.

Chemical Synthesis of Peptides: *General Procedure*. The peptides were synthesized on a continuous flow PerSeptive Biosystems Pioneeer solid-phase synthesizer using the Fmoc/^{t}Bu protection strategy (*22*) with NovaSyn PR-500 resin at 0.2 mmol scale. Single coupling cycles of 30 min with OPfp/HOBt chemistry were employed for all amino acids. The side chain protecting groups used are as follows: Lys (^{t}-Boc); Glu (O^{t}Bu); Cys (Trt); His (^{t}Boc); Arg (Pmc). After peptide assembly the N-termini were manually acetylated followed by thorough washing with DMF, MeOH, and CH_2-Cl_2. Each peptide was cleaved from the resin and simultaneously deprotected using 90:8:2 (v/v/v) trifluoroacetic acid−ethanedithiol−water for 3 h. Crude peptides were precipitated and washed with cold ether, followed by dissolution in water (0.1% v/v TFA), lyophilization, and reversed-phase C_{18} HPLC purification to homogeneity using aqueous acetonitrile gradients containing 0.1% (v/v) TFA. The N-terminal cysteine residues of the purified peptides were air oxidized to the symmetric disulfides in 100 mM ammonium carbonate buffer, pH 9.5 (4−7 h), which was followed by analytical HPLC. After lyophilization, the identities of the resulting di-α-helical disulfide-bridged peptides were confirmed with laser desorption mass spectrometry.

Solution Molecular Weight Determination. Analytical size exclusion chromatography was performed on a Beckman System Gold HPLC system (Fullerton, CA) with a diode array detector using a Pharmacia Superdex 75 column (Pharmacia Biotech, Uppsala, Sweden) eluted with aqueous buffer (10 mM KP_i, 100 mM KCl, pH 8.0) at a flow rate of 0.5 mL/min. The column was standardized with the globular proteins (MW): aprotinin (6.5 kDa), horse heart cytochrome *c* (12.1 kDa), ribonuclease A (13.7 kDa), myoglobin (16.7 kDa), chymotrypsinogen (25.0 kDa), ovalbumin (43.0 kDa), and bovine serum albumin (67.0 kDa).

Circular Dichroism Spectropolarimetry. CD spectra were recorded on an AVIV 62DS spectropolarimeter using rectangular quartz cells of 2 mm path length with a 10 s averaging time. Thermal control was maintained by a thermoelectric module with a Neslab CFT-33 refrigerated recirculating water bath. Peptide concentrations were between 3.5 and 4.0 μM (four-helix bundle) as determined spectrophotometrically using ϵ_{280} of 5600 M^{-1} cm^{-1} $helix^{-1}$.

Denaturation Studies. Peptide denaturation curves at 25 °C were fit to a dimer folded to two monomer unfolded equilibrium using a nonlinear least squares routine in KaleidaGraph (Abelbeck Software) to the equation (*23*):

$$\text{fraction folded} = 1 - (\exp(-\Delta G_{unf}/RT)/4P)[(1 + 8P/\exp(-\Delta G_{unf}/RT))^{1/2} - 1]$$

where P is the molar concentration of total monomeric protein and $\Delta G_{unf} = \Delta G^{H_2O} - m[\text{Gdn·HCl}]$, m is the cosolvation term, which is a measure of the cooperativity of the transition, and [denaturant] is the concentration of denaturant (M).

UV−Vis Spectroscopy. UV−visible spectra were recorded on a Perkin-Elmer Lambda 2 spectrophotometer using quartz cells of 0.1, 0.2, 1.0, and 10 cm path length. Peptide concentrations were determined spectrophotometrically using ϵ_{280} of 5600 M^{-1} cm^{-1} per helix.

Heme Incorporation. A DMSO solution of hemin was added in 0.1 equiv aliquots to peptide solutions (10 mM KP_i, 100 mM KCl, pH 7.5) with 10 min equilibration between additions. The K_d values were obtained from fitting the absorbance at 412 nm plotted against [heme]/[four-helix bundle] according to an equation for two independent binding sites (*24*).

FPLC Purification of Diheme Peptides. Preparative size exclusion chromatography was utilized to remove DMSO and higher order heme−protein aggregates (<5% total protein) prior to concentration for NMR spectroscopy. Purification was performed on a Beckman System Gold HPLC pump with a diode array detector interfaced with a High Load 16/60 Superdex 75 prep grade column eluted with aqueous buffer (10 mM KP_i, 100 mM KCl, pH 7.5) at a 2 mL/min flow rate. The sample provided a chromatogram consistent with that obtained from the analytical size exclusion column. The four-helix bundle fraction was collected and concentrated in Centriprep-3 centrifugal force concentrators in a Sorval RC-5B centrifuge. Analytical size exclusion chromatography of the concentrated peptides displayed a single species of molecular weight consistent with a four-helix bundle aggregation state.

Redox Potentiometry. Chemical redox titrations (*25*) were performed in an anaerobic cuvette equipped with a platinum working and a calomel reference electrode at 22 °C. Ambient redox potentials (measured against the standard hydrogen electrode) were adjusted by addition of aliquots (<1 μL) of sodium dithionite or potassium ferricyanide. Titrations were performed in 10 mM potassium phosphate and 100 mM KCl, pH 7.5. Electrode−solution mediation was facilitated by the following mediators at 10 μM concentration: benzyl viologen, 2,6-dihydroxyanthroquinone, 2-hydroxy-1,4-naphthoquinone, anthroquinone-2-sulfonate, duroquinone, phenazine ethosulfate, phenazine methosulfate, pyocyanine, 1,4-benzoquinone, 1,2-naphthoquinone, and 1,4-naphthoquinone. After equilibration at each potential, the optical spectrum was recorded. Reduction of the hemes was followed by the increase in the α-band absorption at 559 nm relative to a baseline wavelength (700 nm) or by the increase in γ-band absorption at 426 nm relative to an isosbestic point (417 nm). Spectral intensity was plotted against potential, and the data were fit to either a single or a pair of Nernst equations of equal weight with $n = 1.0$ (fixed).

NMR Spectroscopy. Apopeptide one-dimensional proton spectra were acquired on a INOVA-600 spectrometer: spectral width 7200 Hz (12 ppm); t_{max} 142 ms; apodization function cosine, 15° shifted; zero-filling 4096 points. The apopeptide samples were prepared at 500 μM monomer concentration (250 μM four-helix bundle) in 20 mM phosphate (pH 7.25), 50 mM KCl, and 8% D_2O. Heme-loaded peptide NMR spectra were acquired on a Varian INOVA-500 spectrometer: spectral width 15 000 Hz (30 ppm); t_{max} 136 ms; apodization function cosine, 15° shifted; zero-filling 4096 points. Heme-loaded samples were prepared at 250 μM four-helix bundle concentration in 20 mM KP_i, 50 mM KCl, and 8% D_2O at pH 6.6. All proton chemical shifts were referenced to an external sample of DSS at 0.00 ppm. The NMR data were processed on SGI computers using FELIX95 software (Molecular Simulations, San Diego, CA).

RESULTS

Design of $[I_6F_{13}H_{24}]_2$ Variants. The first conformationally unique member of the $(\alpha\text{-SS-}\alpha)_2$ architectural class, $[I_6F_{13}H_{24}]_2$, was derived from the multistructured prototype heme protein maquette, $[L_6L_{13}H_{24}]_2$, previously called $[H10H24]_2$ (*1*). An iterative redesign process based on the replacement of flexible leucine residues with more rigid β-branched and aromatic amino acids was developed and provided a conformational specificity map of sequence space (*3*, *21*). The exact pathway in sequence space was as follows:

$[L_6L_{13}H_{24}]_2 \rightarrow$
(multistructured)
$[I_6L_{13}H_{24}]$ or $[L_6F_{13}H_{24}]_2 \rightarrow$
(two dominant structures) or (uniquely structured)
$[I_6F_{13}H_{24}]_2$
(uniquely structured)

Each arrow represents a single amino acid alteration per helix or four alterations per four-helix bundle. The nativelike character of $[I_6F_{13}H_{24}]_2$, representative of the generic $(\alpha\text{-SS-}\alpha)_2$ class of maquette scaffolds, in the apo state was determined by NMR spectroscopy (*2*). Recently, the solution structure of the disulfide-bridged di-α-helical monomer, $(\alpha\text{-SS-}\alpha)$, of this second generation apomaquette scaffold has been completed by NMR methodologies (*20*, *21*). Furthermore, the relative orientations of the two di-α-helical subunits were deduced to be anti (loops on opposite sides of the four-helix bundle) by the chemical attachment of optical and fluorescence probes (*26*).

One result from the solution structure shown in Figure 1 is that the tight hydrophobic packing in the vicinity of the heme ligands precludes a heme binding pocket as observed in globular heme proteins, e.g., myoglobin (*27*). Despite the absence of cavities to accommodate the heme macrocycle, $[I_6F_{13}H_{24}]_2$ binds four hemes with high affinity, two with K_d values of 10−200 nM and two with K_d values of 5−15 μM. However and perhaps as a consequence of tight hydrophobic packing in the apo state, incorporation of the four heme macrocycles leads to multistructured heme proteins due to reorganization of the hydrophobic core (*21*). The complexity of the heme binding and potentiometry data for tetraheme $[I_6F_{13}H_{24}]_2$ prevented site-specific assignment of the individual heme binding constants and reduction potentials of the four heme binding sites, two at positions 10 and two at positions 24.

Variants of $[I_6F_{13}H_{24}]_2$ were designed to remove the two heme binding sites at positions H24 to simplify assignment to the remaining H10 heme data while maintaining the conformational specificity of the apo state. The H24 heme binding sites were selected for replacement since these have a 50-fold weaker affinity for heme in $[L_6L_{13}H_{24}]_2$ compared to the N-terminal H10 site (*1*). The amino acid substitutions (Ala, Ile, and Phe) were chosen for His because they (i) are hydrophobic, (ii) occupy different volumes, and (iii) cannot coordinate iron. The side chain of alanine is a single methyl group that occupies an 88 Å^3 volume and has a high helical propensity (*28*). The β-branched amino acid isoleucine (volume of 166 Å^3) has a *sec*-butyl functionality, and the aromatic amino acid phenylalanine (volume of 190 Å^3) has a benzyl group. Thus, a stepwise series of hydrophobes with

Scheme 1: Sequence Space Representation of the Peptide Variants Studied[a]

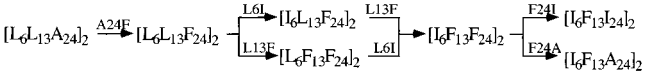

$[L_6L_{13}A_{24}]$	Ac-CGGGE**L**^{6}WKL**H**^{10}EE**L**^{13}LKKFEELLKL**A**^{24}EERLKKL-$CONH_2$ Ac-CGGGE**L**^{6}WKL**H**^{10}EE**L**^{13}LKKFEELLKL**A**^{24}EERLKKL-$CONH_2$
$[L_6L_{13}F_{24}]$	Ac-CGGGE**L**^{6}WKL**H**^{10}EE**L**^{13}LKKFEELLKL**F**^{24}EERLKKL-$CONH_2$ Ac-CGGGE**L**^{6}WKL**H**^{10}EE**L**^{13}LKKFEELLKL**F**^{24}EERLKKL-$CONH_2$
$[I_6L_{13}F_{24}]$	Ac-CGGGE**I**^{6}WKL**H**^{10}EE**L**^{13}LKKFEELLKL**F**^{24}EERLKKL-$CONH_2$ Ac-CGGGE**I**^{6}WKL**H**^{10}EE**L**^{13}LKKFEELLKL**F**^{24}EERLKKL-$CONH_2$
$[L_6F_{13}F_{24}]$	Ac-CGGGE**L**^{6}WKL**H**^{10}EE**F**^{13}LKKFEELLKL**F**^{24}EERLKKL-$CONH_2$ Ac-CGGGE**L**^{6}WKL**H**^{10}EE**F**^{13}LKKFEELLKL**F**^{24}EERLKKL-$CONH_2$
$[I_6F_{13}F_{24}]$	Ac-CGGGE**I**^{6}WKL**H**^{10}EE**F**^{13}LKKFEELLKL**F**^{24}EERLKKL-$CONH_2$ Ac-CGGGE**I**^{6}WKL**H**^{10}EE**F**^{13}LKKFEELLKL**F**^{24}EERLKKL-$CONH_2$
$[I_6F_{13}A_{24}]$	Ac-CGGGE**I**^{6}WKL**H**^{10}EE**F**^{13}LKKFEELLKL**A**^{24}EERLKKL-$CONH_2$ Ac-CGGGE**I**^{6}WKL**H**^{10}EE**F**^{13}LKKFEELLKL**A**^{24}EERLKKL-$CONH_2$
$[I_6F_{13}I_{24}]$	Ac-CGGGE**I**^{6}WKL**H**^{10}EE**F**^{13}LKKFEELLKL**I**^{24}EERLKKL-$CONH_2$ Ac-CGGGE**I**^{6}WKL**H**^{10}EE**F**^{13}LKKFEELLKL**I**^{24}EERLKKL-$CONH_2$
$[I_6F_{13}H_{24}]$	Ac-CGGGE**I**^{6}WKL**H**^{10}EE**F**^{13}LKKFEELLKL**H**^{24}EERLKKL-$CONH_2$ Ac-CGGGE**I**^{6}WKL**H**^{10}EE**F**^{13}LKKFEELLKL**H**^{24}EERLKKL-$CONH_2$

[a] Sequences given in single amino acid code. Each arrow represents the single amino acid modification shown.

volumes smaller than and larger than histidine (153 Å^3) were evaluated to determine the optimal amino acid replacement at this internal protein site (heptad *a* position) in terms of apo state conformational specificity.

The position 24 variant with phenylalanine, $[I_6F_{13}F_{24}]_2$, is conformationally specific (vide infra) and only three amino acids per helix different than the well-characterized prototype $[L_6L_{13}A_{24}]_2$. A series of modified versions of $[L_6L_{13}A_{24}]_2$ were made to link it to $[I_6F_{13}F_{24}]_2$ by a path in sequence space as shown in Scheme 1. Starting with $[L_6L_{13}A_{24}]_2$, phenylalanines replaced the alanines at positions 24 yielding $[L_6L_{13}F_{24}]_2$, a single variant per helix (four per bundle). Second, in $[L_6L_{13}F_{24}]_2$, the leucines at positions 6 were changed to isoleucines ($[I_6L_{13}F_{24}]_2$) or the leucines at positions 13 were changed to phenylalanines ($[L_6F_{13}F_{24}]_2$), each a double variant per helix. Lastly, the path in sequence space was completed by incorporation of all three modifications per helix, yielding the triple variant $[I_6F_{13}F_{24}]_2$. These stepwise modifications provide a continuous path in sequence space on which to map heme properties from $[L_6L_{13}A_{24}]_2$ to $[I_6F_{13}F_{24}]_2$: $[L_6L_{13}A_{24}]_2 \rightarrow [L_6L_{13}F_{24}]_2 \rightarrow [I_6L_{13}F_{24}]_2$ or $[L_6F_{13}F_{24}]_2 \rightarrow [I_6F_{13}F_{24}]_2$, where each arrow represents a single amino acid alteration per helix. These peptides potentially offer insight into the effects that single amino acid alterations per helix can have on heme binding, heme electrochemistry, and apoprotein conformational specificity. Additionally, the apo state conformational specificity evident in these variants of $[L_6L_{13}A_{24}]_2$ can be directly compared to a similar sequence space pathway from $[L_6L_{13}H_{24}]_2$ to $[I_6F_{13}H_{24}]_2$ to ascertain if the two related sequences respond to identical modifications in a similar fashion.

Peptide Aggregation States. The association state of each of the variants of $[I_6F_{13}H_{24}]_2$ was evaluated in the apo and diheme states using gel permeation chromatography with initial loading concentrations ranging from 10 to 100 μM. At all concentrations studied by gel permeation chromatography, the apopeptides elute with apparent molecular masses between 15.9 and 18.6 kDa (calculated M_r of 15.0−15.3 kDa)

Table 1: Peptide Characterization

peptide	molecular weight: monomer mass	molecular weight: gel permeation apo	molecular weight: gel permeation diheme	molar ellipticity (222 nm) (deg cm^{-2} dmol^{-1}): apo	molar ellipticity (222 nm) (deg cm^{-2} dmol^{-1}): diheme	% α-helix: apo	% α-helix: diheme	$[Gdn\cdot HCl]_{1/2}$ (M)	$-\Delta G^{H_2O}$ (kcal mol^{-1})	m (kcal mol^{-1} M^{-1})
$[L_6L_{13}A_{24}]_2$	7444	18 600	19 200	26 100	27 100	81.5	84.6	5.59	24.8	3.1
$[L_6L_{13}F_{24}]_2$	7512	16 200	17 400	26 400	28 000	82.5	87.5	6.9 (estd)	>30 (estd)	>3 (estd)
$[I_6L_{13}F_{24}]_2$	7512	16 700	18 200	24 800	27 200	77.5	85.0	6.51	26.7	2.9
$[L_6F_{13}F_{24}]_2$	7578	17 100	18 000	26 600	26 900	83.2	84.1	6.9 (estd)	>30 (estd)	>4 (estd)
$[I_6F_{13}F_{24}]_2$	7664	16 400	17 600	27 800	29 500	86.9	92.1	6.48	35.7	4.3
$[I_6F_{13}A_{24}]_2$	7512	16 700	18 200	27 800	28 400	86.9	88.7	4.28	20.4	3.0
$[I_6F_{13}I_{24}]_2$	7596	15 900	17 800	25 000	26 700	78.1	83.4	5.22	21.2	2.7

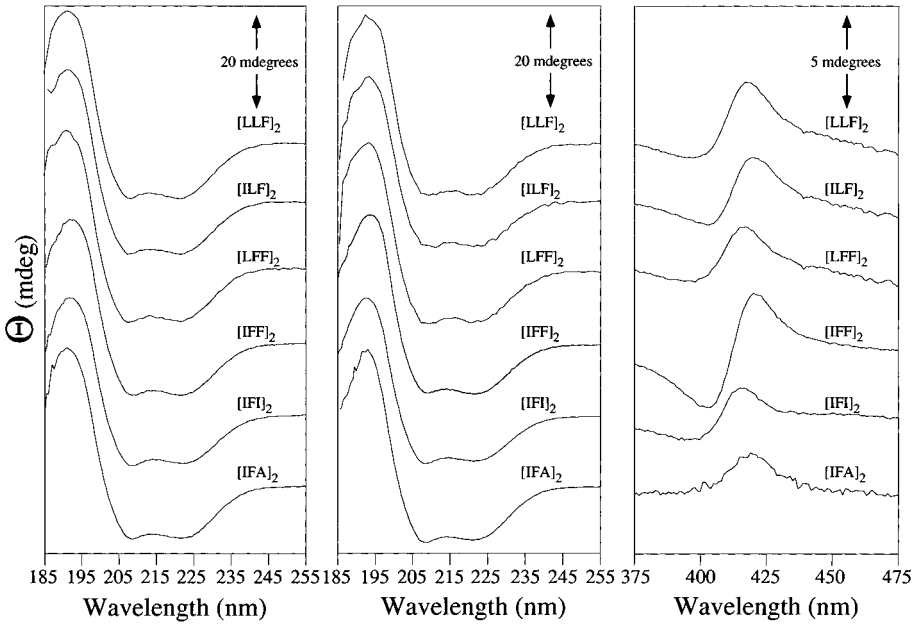

FIGURE 2: CD spectral comparison of the position 24 variants of $[I_6F_{13}H_{24}]_2$ followed by circular dichroism spectropolarimetry recorded at 25 °C in 10 mM potassium phosphate and 100 mM KCl, pH 7.5, buffer. The peptides were investigated in both the apo (left panel) and diheme states (center panel) which were also studied in the visible region of the spectrum (right panel). Peptide concentrations were 4.5 μM four-helix bundle as determined spectrophotometrically using Trp (ϵ_{280} = 5600 M^{-1} cm^{-1}) or oxidized heme (ϵ_{412} = 120 mM^{-1} cm^{-1}).

based on a column standardization curve derived from data on globular proteins as shown in Table 1. These peptides coelute with the $[I_6F_{13}H_{24}]_2$, known to be a four-helix bundle by analytical ultracentrifugation, size exclusion chromatography, translational diffusion, and rotational correlation time (τ_c) measurements (*21*). In the diheme state, the peptides elute with slightly larger apparent molecular masses, 17.4−19.2 kDa (calculated M_r of 16.2−16.5 kDa), consistent with the incorporation of two heme moieties (0.6 kDa each). The data show that neither conservative amino acid substitutions nor the incorporation of two hemes results in disruption of the designed dimeric aggregation state.

Peptide Secondary Structure. The left panel of Figure 2 shows the far-UV CD spectra of each of the apo state $[I_6F_{13}H_{24}]_2$ variants in aqueous buffer which are typical of highly α-helical peptides (77−87% helical content) with minima at 208 and 222 nm ($\pi \rightarrow \pi^*$ and n $\rightarrow \pi^*$ minimum of α-helical systems, respectively) and a maximum at 192 nm. The center panel of Figure 2 shows the far-UV CD spectra of the diheme peptides that are characteristic of a highly α-helical framework. The calculated helicities of the diheme peptides (83−92% helicity) provide only an estimate of the helical content, as the heme macrocycle may have induced CD bands in this spectral region; however, it is clear that there is no major change in the peptide secondary structure upon heme incorporation.

Thermodynamic Stability. Figure 3 shows the chemical denaturation of the peptides in the apo state as observed by circular dichroism spectropolarimetry (*29*). Prior to addition of guanidine hydrochloride, the mean residue ellipticities at 222 nm ($[\Theta]_{222}$) for the peptides studied are all greater than −25 000 deg cm^2/dmol, consistent with the design. Upon addition of molar concentrations of guanidine hydrochloride, $[\Theta]_{222}$ approaches zero, indicating protein denaturation to form random coil structures for each of the position 24 variants as well as for $[I_6L_{13}F_{24}]_2$. These cooperative denaturation curves are sigmoidal with single inflection points, consistent with a two-state equilibrium in which any intermediates are minimally populated at equilibrium. $[L_6F_{13}F_{24}]_2$ and $[L_6L_{13}F_{24}]_2$ are resistant to chemical denaturation at 25 °C, and there exists a significant population of native state in saturated guanidine hydrochloride. Table 1 illustrates that the midpoint of the denaturation curves ($[Gdn]_{1/2}$), molar cosolvation terms (m), and $-\Delta G^{H_2O}$ values derived assuming a two-state model were highly dependent on the identity of the modification made to the four helices. All of the peptides are highly stable in the apo state with $-\Delta G^{H_2O}$ values ranging from 20 kcal/mol for $[I_6F_{13}A_{24}]_2$ to 35 kcal/mol for $[I_6F_{13}F_{24}]_2$.

Conformational Specificity. Figure 4 shows the one-dimensional ^{1}H NMR spectrum of the apo state variants of $[I_6F_{13}H_{24}]_2$, whose NMR solution structure has been solved

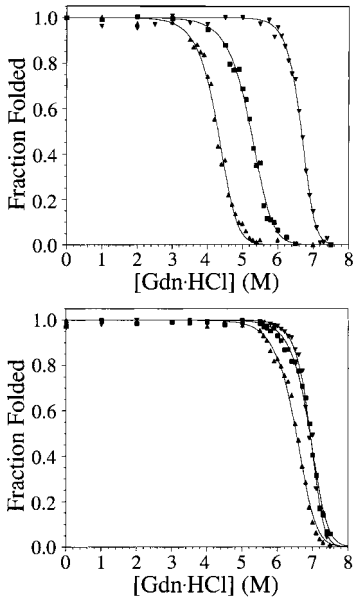

FIGURE 3: Guanidine hydrochloride denaturation melts of the $[I_6F_{13}H_{24}]_2$ variants (top panel) $[I_6F_{13}A_{24}]_2$ (▲), $[I_6F_{13}I_{24}]_2$ (■), and $[I_6F_{13}F_{24}]$ (▼) and (bottom panel) $[L_6L_{13}F_{24}]_2$ (▲), $[I_6L_{13}F_{24}]_2$ (■), and $[L_6F_{13}F_{24}]_2$ (▼), followed by circular dichroism spectropolarimetry recorded at 25 °C in 10 mM potassium phosphate and 100 mM KCl, pH 8.0, buffer. Peptide concentrations were 7.5 μM (1.9 μM four-helix bundle) as determined spectrophotometrically using Trp (ϵ_{280} = 5600 M^{-1} cm^{-1} $helix^{-1}$).

(*21*). Multiplicity of structure is clearly indicated for $[I_6F_{13}I_{24}]_2$ and $[I_6F_{13}I_{24}]_2$ as their aromatic and amide ^1H resonances exhibit larger line widths consistent with a manifold of interconverting conformations in the slow to intermediate exchange range on the ^1H chemical shift time scale (milliseconds). Nonspecific protein aggregation, also consistent with the observed line widths, does not occur (vide supra). However, the ^1H NMR spectrum of $[I_6F_{13}F_{24}]_2$ is fully consistent with a highly populated singular solution conformation showing not only narrow ^1H resonance line widths but also large amide, aromatic, and methyl proton chemical shift dispersion. This spectrum is similar in quality to that of the uniquely structured $[I_6F_{13}H_{24}]_2$. These spectra indicate that the substitution of H24 with F24 in $[I_6F_{13}H_{24}]_2$ results in a peptide with retention of conformational specificity, suggesting that aromatic hydrophobes are best accommodated in this sequence position.

Figure 4 also illustrates the conformational specificity of the apo form maquettes in the stepwise transition from the multistructured prototype, $[L_6L_{13}A_{24}]_2$, to the single structured $[I_6F_{13}H_{24}]_2$. Starting from $[L_6L_{13}A_{24}]_2$, incorporation of a phenylalanine at position 24, $[L_6L_{13}F_{24}]_2$, yields a dramatic increase in the resolution of the NMR spectrum. The two double per helix variants of $[L_6L_{13}A_{24}]_2$, $[I_6L_{13}F_{24}]_2$ and $[L_6F_{13}F_{24}]_2$, and the triple per helix variant, $[I_6F_{13}F_{24}]_2$, yield NMR spectra consistent with singlular solution conformations. These data demonstrate that single hydrophobic core modifications per helix (four per bundle) are responsible for the transformation of a multistructured peptide into a uniquely structured scaffold. The conformational specificity outcomes of these core modifications coincide with those observed for the conversion of the related multistructured tetraheme prototype, $[L_6L_{13}H_{24}]_2$, into the uniquely structured $[I_6F_{13}H_{24}]_2$. Thus, the same sequence to conformational specificity relationship holds for the maquette scaffold

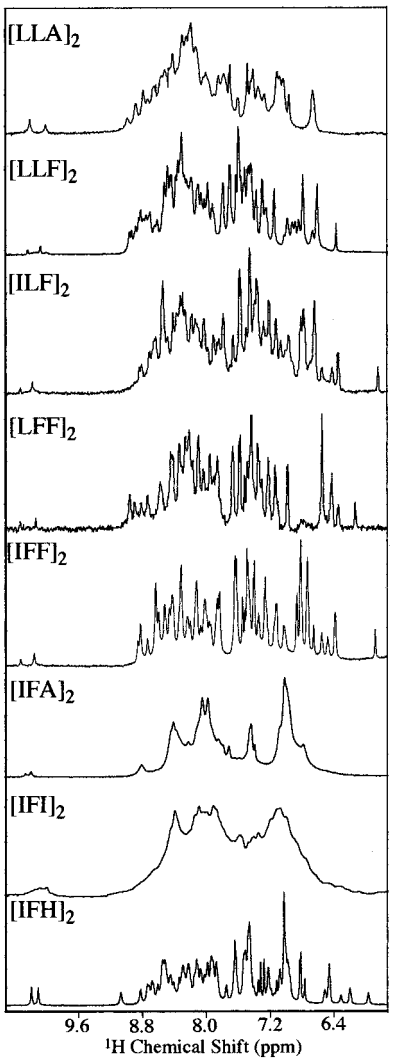

FIGURE 4: One-dimensional NMR spectra in the aromatic−amide regions of all apo-$[I_6F_{13}H_{24}]_2$ variants studied: (A) apo-$[L_6L_{13}A_{24}]_2$, (B) apo-$[L_6L_{13}F_{24}]_2$, (C) apo-$[I_6L_{13}F_{24}]_2$, (D) apo-$[L_6F_{13}F_{24}]_2$, (E) apo-$[I_6F_{13}F_{24}]_2$, (F) apo-$[I_6F_{13}I_{24}]_2$, (G) apo-$[I_6F_{13}A_{24}]_2$, and (H) apo-$[I_6F_{13}H_{24}]_2$. Spectra were acquired using identical acquisition and processing parameters.

regardless of the position 24 occupant, histidine or phenylalanine. This hints that sequence−structure information acquired from one maquette scaffold may be transferable to another related scaffold, a concept not previously demonstrated in de novo design.

Ferric Heme−Peptide Dissociation Constants. Measurements to determine the individual K_d values for the variants of $[I_6F_{13}H_{24}]_2$ were performed over the peptide concentration range of 35 nM to 2 μM. Figure 5A,B illustrates by UV−visible spectroscopy that the histidine to isoleucine variant, $[I_6F_{13}I_{24}]_2$, binds only two hemes consistent with the removal of the two H24 heme binding sites in $[IFH]_2$. Titration of 100 nM hemin [ferric(protoporphyrin IX)Cl] in DMSO into aqueous solutions of 48 nM, 720 nM, and 1.72 μM peptide (10 mM KP_i, 100 mM KCl, pH 7.5) with gentle agitation results in facile incorporation of heme into $[I_6F_{13}I_{24}]_2$ as evidenced by increase in the Soret maximum at 412 nm (ϵ of 1.20 × 10^5 M^{-1} cm^{-1} $heme^{-1}$) and poorly resolved α- and β-bands at 535 nm. After addition of each aliquot, equilibration is complete within 5 min. Two independent K_d values for the pair of H10 binding sites of $[I_6F_{13}I_{24}]_2$ were

Table 2: Properties of Heme Proteins

	heme optical spectroscopy λ_{max}, nm (ϵ, mM^{-1} cm^{-1})		heme dissociation constant		heme reduction potential ($E_{m7.5}$ in mV vs SHE)		$\Delta E_{m7.5}$ (mV)
peptide	oxidized	reduced	K_{d1} (nM)	K_{d2} (nM)	one heme	two hemes	two hemes
$[L_6L_{13}A_{24}]_2$	412 (120) 535 (13.2)	426 (140) 529 (16.0) 559 (27.0)	50	800	−156[a]	−144[a] −216[a]	72[a]
$[L_6L_{13}F_{24}]_2$	412 (122) 535 (13.0)	426 (134) 529 (14.0) 559 (24.7)	65	700	−168	−156 −228	72
$[I_6L_{13}F_{24}]_2$	412 (120) 535 (12.5)	426 (135) 529 (12.2) 559 (21.1)	<0.5	200	−203	−202	0
$[L_6F_{13}F_{24}]_2$	412 (124) 535 (13.1)	426 (139) 529 (13.8) 559 (23.5)	<0.5	150	−204	−202	0
$[I_6F_{13}F_{24}]_2$	412 (121) 535 (13.5)	426 (133) 529 (13.6) 559 (26.6)	<0.5	150	−210	−150 −276	126
$[I_6F_{13}A_{24}]_2$	412 (123) 535 (13.9)	426 (137) 529 (14.2) 559 (23.1)	<0.5	35	−208	−158 −262	104
$[I_6F_{13}I_{24}]_2$	412 (120) 535 (13.3)	426 (143) 529 (13.3) 559 (25.6)	<0.5	130	−191	−156 −288	132

[a] E_{m8} reduction potentials taken from ref *52*.

determined to be at <0.5 nM and 130 nM, shown as insets to Figure 5A,B; similar values are measured for $[I_6F_{13}F_{24}]_2$. The alanine variant, $[I_6F_{13}A_{24}]_2$, has a 4-fold weaker heme affinity. The similarity of these K_d values to the tight binding site K_d values of the four-heme parent, $[I_6F_{13}H_{24}]_2$, allows their assignment to the H10 positions in the parent. Furthermore, the K_d values at position H10 show a slight modulation, <5-fold, by the identity of the hydrophobic amino acid at 24,24′. Reduction of diheme $[I_6F_{13}I_{24}]_2$ with sodium dithionite results in a heme optical spectrum with a Soret maximum at 426 nm ($\epsilon = 1.43 \times 10^5$ M^{-1} cm^{-1} $heme^{-1}$) and a well-resolved β-band at 529 nm ($\epsilon = 1.3 \times 10^4$ M^{-1} cm^{-1} $heme^{-1}$) with an α-band at 559 nm ($\epsilon = 2.6 \times 10^4$ M^{-1} cm^{-1} $heme^{-1}$), values representative of the series enumerated in Table 2 and typical of bishistidine ligated *b*-type cytochromes (*30*).

The individual K_d values of the sequence space pathway peptides were determined to ascertain the amino acid changes which resulted in the observed increase in heme affinity. The substitution of a phenylalanine at position 24 in $[L_6L_{13}A_{24}]_2$ resulted in no significant alteration in heme affinity, K_{d1} of 65 nM and K_{d2} of 700 nM for $[L_6L_{13}F_{24}]_2$. In contrast, the incorporation of either an isoleucine at position 6 or a phenylalanine at position 13 resulted in roughly a 10-fold tighter affinity for the first heme and a 4-fold tighter affinity for the second heme, K_{d1} of <0.5 nM and K_{d2} of 150−200 nM. Clearly, conservative amino acid changes local to the heme binding histidines at positions 10 can affect the heme affinity by up to an order of magnitude. The peptide containing all three amino acid modifications, $[I_6F_{13}F_{24}]_2$, retained the tight heme binding properties established in the double variants.

Induced Circular Dichroism of the Diheme Peptides. The right panel of Figure 2 illustrates the induced CD of the heme upon incorporation into the peptide scaffold. This series of spectra demonstrate that the hemes reside in chiral environments since monomeric hemes in isotropic solution show no circular dichroism (*31*). The visible CD of the peptide variants at positions 6 and 13, local to the heme binding histidines at positions 10, show nearly identical circular dichroism spectra. The similar Cotton effects observed for $[L_6L_{13}F_{24}]_2$, $[I_6L_{13}F_{24}]_2$, and $[L_6F_{13}F_{24}]_2$ illustrate comparable heme distortions within the peptides despite changes in hydrophobic amino acids close to the heme macrocycle. In contrast, the hemes bound to $[I_6F_{13}A_{24}]_2$, $[I_6F_{13}I_{24}]_2$, and $[I_6F_{13}F_{24}]_2$ peptides each reside in distinct local environments despite the fact that the amino acid differences lie >20 Å away from the H10 heme binding sites. The CD spectrum of diheme $[I_6F_{13}A_{24}]_2$ displays a weak positive Cotton effect at 412 nm, the λ_{max} of the heme Soret absorption. A more intense and somewhat asymmetric circular dichroism spectrum is observed for diheme $[I_6F_{13}I_{24}]_2$ which is similar to that observed for $[L_6L_{13}F_{24}]_2$, $[I_6L_{13}F_{24}]_2$, and $[L_6F_{13}F_{24}]_2$. The Soret CD spectrum of diheme $[I_6F_{13}F_{24}]_2$ is S-shaped, displaying a splitting into two approximately equal and opposite bands. While the diheme $[I_6F_{13}F_{24}]_2$ spectrum is suggestive of heme−heme excitonic interaction (*32*), the CD spectrum of monoheme $[I_6F_{13}F_{24}]_2$ (data not shown), known to be a four-helix bundle containing a single heme, is identical in line shape and position, demonstrating that this mechanism is unlikely. The data for diheme $[I_6F_{13}X_{24}]_2$ (X = A, I, F) are consistent with a lowering of the heme symmetry with concomitant loss of the double degeneracy of the Soret transition in response to the increasing steric bulk of the hydrophobic residue at position 24 which also affects the apopeptide conformational specificity as shown by NMR spectroscopy. The lower symmetry of the Soret between diheme $[I_6F_{13}F_{24}]_2$ and diheme $[I_6F_{13}A_{24}]_2$, as evidenced by CD, illustrates significant distortions in heme conformation at the H10 binding sites due to remote hydrophobic amino acids (*33*). Since the hemes in all of these diheme peptides are proximial to aromatic residues, variable steric constraints and hydrophobic packing at position 24 may aid in the observed heme distortions. Additionally, adjustable coupling of the heme $\pi \rightarrow \pi^*$ electric dipole transition (*34*) with phenylalanine 13 in these peptides may serve as the mechanism for increasing the rotational strength observed in the induced CD spectra.

Conformational Uniqueness of the Diheme State. Figure 6 shows the impact of ferric heme incorporation on the NMR spectrum of the peptides. The extraordinarily large ^1H

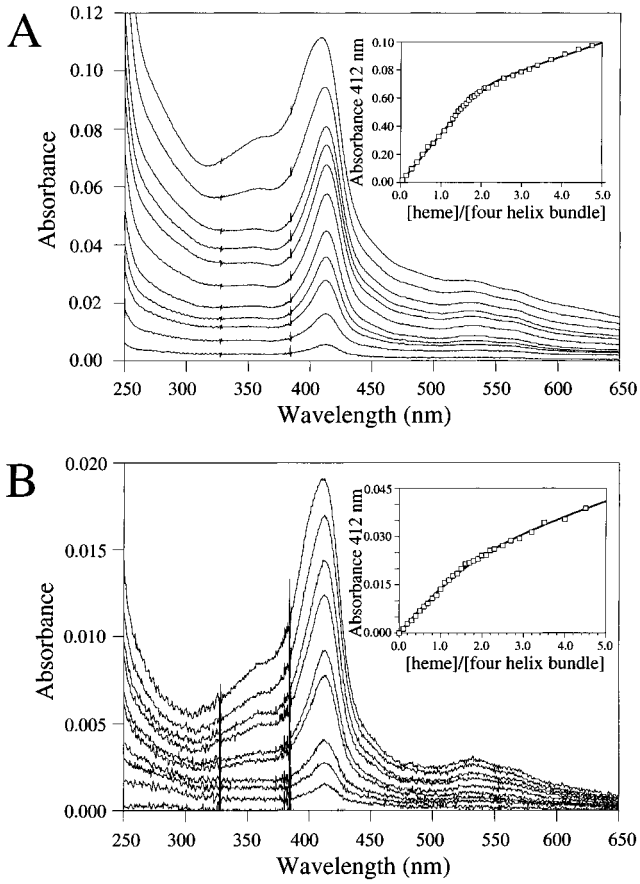

FIGURE 5: Heme binding isotherms for $[I_6F_{13}I_{24}]_2$. (A) Titration of a DMSO solution of hemin into a 720 nM peptide (360 nM $[I_6F_{13}I_{24}]_2$ solution recorded in a 1 cm path-length cuvette at 25 °C. Spectra shown contain 0.13, 0.41, 0.68, 0.95, 1.22, 1.49, 1.76, 2.06, 2.57, 3.38, and 4.74 equiv of added hemin per four-helix bundle. The increasing absorbance at 250 nm is due to DMSO. (B) Titration of hemin into a 48 nM peptide (24 nM $[I_6F_{13}I_{24}]_2$) solution recorded in a 10 cm path-length cuvette at 25 °C. Spectra shown contain 0.0, 0.2, 0.4, 0.6, 0.7, 0.8, 0.9, 1.0, 1.2, and 1.4 equiv of added hemin per four-helix bundle. Insets display the absorbance at 412 nm versus [heme]/[four-helix bundle] ratio titration curve with fits.

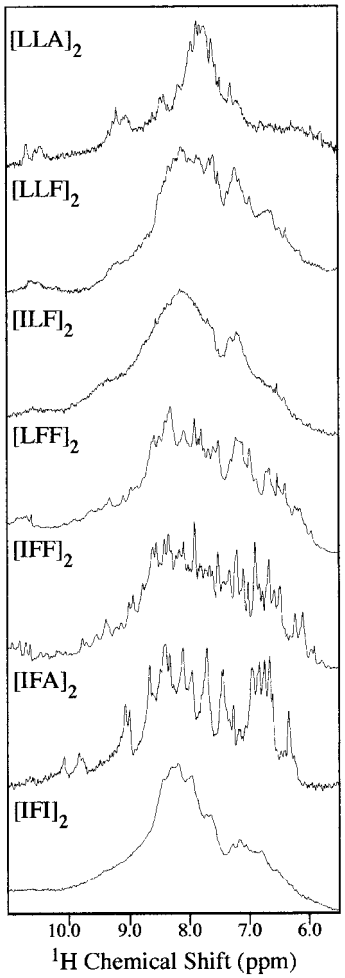

FIGURE 6: One-dimensional NMR spectra in the aromatic−amide regions of all the oxidized diheme peptides studied: (A) diheme $[L_6L_{13}A_{24}]_2$, (B) diheme $[L_6L_{13}F_{24}]_2$, (C) diheme $[I_6L_{13}F_{24}]_2$, (D) diheme $[L_6F_{13}F_{24}]_2$, (E) diheme $[I_6F_{13}F_{24}]_2$, (F) diheme $[I_6F_{13}A_{24}]_2$, and (G) diheme $[I_6F_{13}I_{24}]_2$. Spectra were acquired using identical acquisition and processing parameters.

resonance line widths observed can arise from paramagnetic relaxation, nonspecific aggregation, or generation of multiple, yet slowly, interconverting conformations. Since aggregation has been ruled out by size exclusion chromatography and a variety of other analytical techniques, we surmise that incorporation of heme is a disorganizing global influence on the highly packed apo conformation leading to a multi-structured holopeptide ensemble. The majority of diheme maquettes are clearly multistructured in solution, but two of the peptides, $[I_6F_{13}A_{24}]_2$ and $[I_6F_{13}F_{24}]_2$, possess one-dimensional proton NMR spectra which have some relatively narrow line-width resonances and slightly greater amide, aromatic, and methyl proton chemical shift dispersion. The NMR spectra of diheme $[I_6F_{13}A_{24}]_2$ and diheme $[I_6F_{13}F_{24}]_2$ suggest a first step toward the quality of spectra necessary for solution structure determination. While these current designs do not lend themselves to direct solution NMR structural investigation, iterative redesign of $[I_6F_{13}A_{24}]_2$ or $[I_6F_{13}F_{24}]_2$ may yield single-structured holoproteins.

Heme Redox Potentiometry. Monoheme State. The electrochemical reduction midpoint potential of a single bound heme in each of the peptides was determined by monitoring the changes in the α-, β-, and γ-bands of the heme absorption spectra as a function of redox potential. Figure 7 shows the redox titration of monoheme $[I_6F_{13}F_{24}]_2$ which is fit to a single $n = 1$ Nernst curve with a midpoint ($E_{m7.5}$) of -210 ± 8 mV vs SHE. The equilibrium reduction midpoint potentials of monoheme $[I_6F_{13}A_{24}]_2$ and $[I_6F_{13}I_{24}]_2$ were determined to be -208 and -191 ± 8 mV, respectively. The value of -208 mV for $[I_6F_{13}A_{24}]_2$ is significantly lower than the reduction potential of monoheme $[L_6L_{13}A_{24}]_2$ ($E_{m7.5}$ value of -156 mV) (*19*), which differs in sequence by two amino acids per helix, positions 6 and 13 are both occupied by leucines in $[L_6L_{13}A_{24}]_2$, and by an isoleucine and a phenylalanine in $[I_6F_{13}A_{24}]_2$. The observation of a lower reduction midpoint potential of the heme for $[I_6F_{13}A_{24}]_2$ compared to $[L_6L_{13}A_{24}]_2$ ($\Delta E_{m7.5}$ of 52 mV) illustrates the effect that local hydrophobic amino acids can have on heme potentials and prompted investigation of the structural connection between these two related peptides by single step amino acid changes per helix.

The electrochemistry of the sequence space pathway variant peptides was also measured to provide insight into the 54 mV lower reduction potential of the heme in $[I_6F_{13}F_{24}]_2$ compared to $[L_6L_{13}A_{24}]_2$. Starting from the prototype, $[L_6L_{13}A_{24}]_2$ ($E_{m7.5}$ of -156 mV vs SHE), incorporation of the phenylalanine at position 24, $[L_6L_{13}F_{24}]_2$, results in a

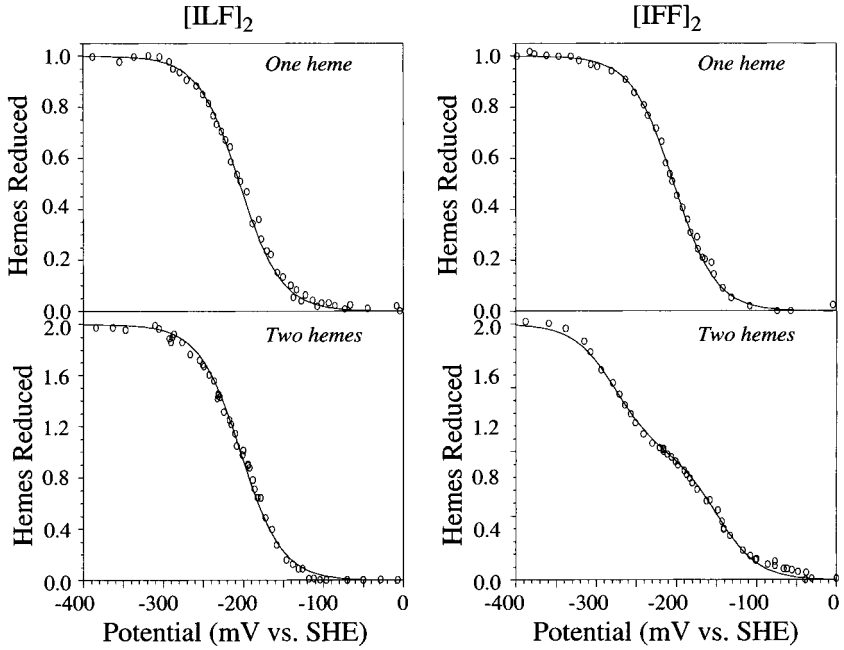

FIGURE 7: Redox titration curves of the one-heme bound (top panels) and two-heme (lower panels) loaded states of $[I_6L_{13}F_{24}]_2$ (left) and $[I_6F_{13}F_{24}]_2$ (right) monitored by optical spectroscopy at 25 °C. The number of hemes reduced was determined by the change in absorbance at 426 nm (γ-band maximum) relative to an isosbestic point (417 nm) normalized to either one or two hemes for the titrations. The solid line represents either a one or a two Nernst equation fit to the experimental data points. Reduction potentials are reported relative to SHE.

slightly lower $E_{m7.5}$ ($E_{m7.5}$ of −168 mV). A consequence of the introduction of *either* second modification per helix, $[I_6L_{13}F_{24}]_2$ or $[L_6F_{13}F_{24}]_2$, is the lowering of the reduction potential to −203 and −204 mV, respectively. These variants illustrate clearly that the principal drop in E_m ($\Delta E_{m7.5}$ of ≈40 mV) results from conservative hydrophobic amino acid changes local to the His10 heme binding site. Taken together, these two examples, $[L_6L_{13}F_{24}]_2$ and $[I_6L_{13}F_{24}]_2$ or $[L_6F_{13}F_{24}]_2$, clearly illustrate the modulation of heme electrochemistry by both long-range (weak) and local (stronger) hydrophobic amino acid changes. When these modifications are combined to yield $[I_6F_{13}F_{24}]_2$, their −35 and −36 mV effects relative to $[L_6L_{13}F_{24}]_2$ are not additive as the reduction potential remains at −210 mV, only a −42 mV change relative to $[L_6L_{13}F_{24}]_2$.

pH Dependence of the Monoheme State. The reduction potential of heme bound to the prototype maquette, $[L_6L_{13}A_{24}]_2$, is pH dependent [the redox−Bohr effect (*35*, *36*)], showing an oxidized pK_a of 4.2 and an reduced pK_a of 7.0. The redox−Bohr effect shows a −60 mV/pH unit slope demonstrating coupling of a single proton to heme reduction (*19*). We investigated the possibility that an alteration in the pK_a of the proton acceptor glutamic acid was responsible for the observed 52 mV lower reduction potential of $[I_6F_{13}A_{24}]_2$ compared to $[L_6L_{13}A_{24}]_2$ by measuring the E_m as a function of pH. Figure 8 compares the pH dependency of $[I_6F_{13}A_{24}]_2$ and $[L_6L_{13}A_{24}]_2$, which yield identical pK_a values within the ±0.2 pH unit precision of the measurement. Furthermore, cyclic voltammetry of a related peptide on a Langmuir−Blodgett monolayer yields similar low potentials (*37*). These data clearly illustrate that the lower $E_{m7.5}$ values of this peptide series are not due to alteration of the glutamic acid pK_a values.

Determining the Global Topology of the Diheme Maquettes. The electrochemistry of the diheme position 24 variant peptides, containing two hemes per four-helix bundle, shows

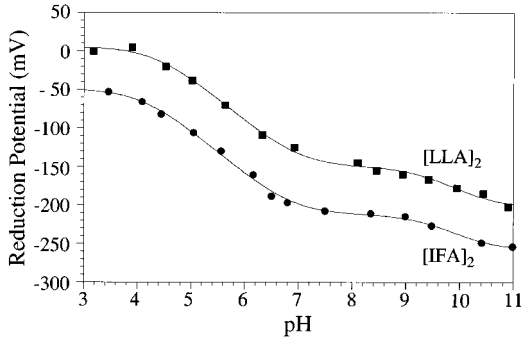

FIGURE 8: pH dependency of the reduction potential versus SHE of the one-heme bound state of $[I_6F_{13}A_{24}]_2$ compared with the prototype, $[L_6L_{13}A_{24}]_2$. Each point represents an independent potentiometric titration at different pH values. The buffers used are given in the text. Fitting of the experimental data points for $[I_6F_{13}A_{24}]_2$ to eq 3 in ref 19 yielded $pK_a^{ox}{}_1 = 4.1$ and $pK_a^{red}{}_1 = 6.8$, $pK_a^{ox}{}_2 = 9.5$ and $pK_a^{red}{}_2 = 10.3$, values similar to those derived for $[L_6L_{13}A_{24}]_2$.

electrostatic perturbation of the midpoint potential of the first heme reduction site by the second heme reduction site which allows for determination of the global topology of the two di-α-helical subunits (*38*). Figure 7 and Table 2 show the equilibrium reduction midpoint potential of diheme $[I_6F_{13}F_{24}]_2$, which clearly demonstrates two equivalent electrochemical events separated by 126 mV due to heme−heme electrostatic interaction. The diheme $[I_6F_{13}F_{24}]_2$ data were fit to a pair of Nernst equations with midpoints ($E_{m7.5}$) of −150 mV and −276 mV (ΔE_m value of 126 mV). Diheme $[I_6F_{13}A_{24}]_2$ and diheme $[I_6F_{13}I_{24}]_2$ show similar behavior with ΔE_m heme−heme electrostatic interactions indicative of a syn bundle topology (loop regions and hence heme binding sites on the same end of the bundle) in contrast to expectations from the NMR structure of apo-$[I_6F_{13}H_{24}]_2$, which has been shown by fluorescence spectroscopy and protein redesign to be in an anti global topology (*26*). Either the substitution of the

histidines with hydrophobic amino acids or incorporation of the heme macrocycles into the hydrophobic core results in the observed change in protein subunit topology. The evaluated reduction potentials for the higher potential hemes of the pair in diheme $[I_6F_{13}A_{24}]_2$, diheme $[I_6F_{13}I_{24}]_2$, and diheme $[I_6F_{13}F_{24}]_2$ were very similar, in the range of −150 to −160 mV. However, the reduction midpoint potentials of the lower potential hemes showed greater difference with $[I_6F_{13}A_{24}]_2$ at −262 mV and both $[I_6F_{13}I_{24}]_2$ and $[I_6F_{13}F_{24}]_2$ at −288 and −279 mV, respectively. Additionally, the E_m values for the single heme bound state of these position 24 variants reside closer to the average of the two E_m values for the diheme peptide. The slightly greater ΔE_m values in $[I_6F_{13}I_{24}]_2$ and $[I_6F_{13}F_{24}]_2$ suggest greater interheme electrostatic interaction caused perhaps by a more hydrophobic protein environment (lower dielectric constant) around the hemes than evident in $[I_6F_{13}A_{24}]_2$ or the prototype $[L_6L_{13}A_{24}]_2$ (*39*).

The global topology of the two heme containing sequence space pathway variant peptides was determined by electrochemistry. The prototype $[L_6L_{13}A_{24}]_2$ is known to be syn with a 80 mV heme−heme electrochemical interaction (1) with a modeled Fe-to-Fe distance of ≈13 Å. Incorporation of the phenylalanine at position 24, $[L_6L_{13}F_{24}]_2$, results in a similar $\Delta E_{m7.5}$ value ($\Delta E_{m7.5}$ of 72 mV), indicating that this peptide remains in the syn global topology. A clear transformation to an anti global topology is demonstrated upon introduction of either second modification per helix, $[I_6L_{13}F_{24}]_2$ or $[L_6F_{13}F_{24}]_2$, whose two heme bound reduction potentials are identical to their one heme bound reduction potentials. In contrast, the triple variant, $[I_6F_{13}F_{24}]_2$, resides in a syn global topology with a heme−heme electrostatic interaction of 129 mV. These data illustrate that single, conservative amino acid changes per helix can have dramatic effects on the global topology of a de novo designed heme binding four-α-helix bundle. Additionally, single amino acid changes which each singly drive a syn to anti topological conversion in combination can synergistically yield a syn bundle.

DISCUSSION

Using a uniquely structured de novo designed four-α-helix bundle apomaquette, $[I_6F_{13}H_{24}]_2$, we have been able to isolate and then investigate the properties of the hemes in the H10 positions by replacement of the histidines at positions H24 with non-heme ligating amino acids. The heme affinity and electrochemistry of these variants identified the tight heme binding sites and the lower redox activity as the H10 sites in the parent $[I_6F_{13}H_{24}]_2$. NMR spectroscopy illustrates that $[I_6F_{13}F_{24}]_2$ is uniquely structured in the apo state, providing a simpler diheme maquette scaffold for future maquette studies. Heme−heme electrostatic splitting of the diheme peptides ($\Delta E_{m7.5} > 70$ mV) demonstrates the syn global topology of the two protein subunits. The position 24 variant proteins demonstrate that hydrophobic residues distant from the heme binding sites can modulate the heme affinity, electrochemistry, and porphyrin conformation. Furthermore, tracing the alteration of the heme affinity and electrochemistry of the prototype, $[L_6L_{13}A_{24}]_2$, via a pathway in sequence space to $[I_6F_{13}F_{24}]_2$ delineates the single amino acid changes responsible for the modulation of the bound hemes allowing for future rational design of heme properties in designed proteins.

Introduction of the heme macrocycle significantly reorganizes the apopeptide hydrophobic core packing shown in Figure 1. The observed effect of heme incorporation on the apomaquettes studied is not surprising given that in native heme proteins the heme macrocycle is critical for global conformational specificity (myoglobin, cytochrome b_{562}) (*40*, *41*) or is integral to the folding process (cytochrome *c*) (*42*). Within our hierarchical strategy for heme protein design, the $[I_6F_{13}F_{24}]_2$ protein derived from this study represents a significant advancement in that the apo state of this protein retains the conformational specificity of the parent peptide, but with only two high-affinity heme binding sites per bundle. Additionally, the diheme $[I_6F_{13}F_{24}]_2$ NMR spectrum suggests it as a starting sequence for future implementation of our iterative redesign protocol.

Single conservative hydrophobic amino acid modifications local to the heme binding site were found to modulate the heme reduction midpoint potential by up to ±50 mV, consistent with the recent findings of Springs et al. using the first generation library of cytochrome b_{562} mutants (*43*). Furthermore, combinations of single amino acid changes do not have an additive effect on the equilibrium midpoint potential. The 35 mV lower $E_{m7.5}$ observed for either $[I_6L_{13}F_{24}]_2$ or $[L_6F_{13}F_{24}]_2$ relative to $[L_6F_{13}F_{24}]_2$ is strikingly similar to the 36 mV drop in the reduction potential of the heme in flavocytochrome b_2 observed upon mutation of L36I which is in van der Waals contact with the heme periphery (*44*) and the A67V mutant of cytochrome b_5 which has a reduction potential lowered by 20 mV (*45*). Furthermore, the combination of the two helix modifications identified as modulating the heme reduction potential, yielding $[I_6F_{13}F_{24}]_2$, does not lower the reduction potential by 70 mV (2 × 35 mV) but rather by only 42 mV, a value equivalent to either single alteration within the error of the measurement. Additionally, the effects of hydrophobic core modifications are distance dependent as the effects of amino acid changes remote from the heme binding site have significant effects on heme properties (ΔE_m of ≈20 mV between $[I_6F_{13}F_{24}]_2$ and $[I_6F_{13}I_{24}]_2$) but smaller when compared to local amino acid changes (ΔE_m of ≈35 mV between $[L_6L_{13}F_{24}]_2$ and $[I_6L_{13}F_{24}]_2$ or $[L_6F_{13}F_{24}]_2$).

Possible mechanisms reported in the literature for the lowering of the E_m in the one heme bound state include distortion of the porphyrin macrocycle (*46*), changes in peptide secondary structure content (*47*), and alterations in local electrostatics (*48*) such as in charge compensation by glutamate residues or increased exposure to solvent (*49*). Heme plane distortion would be expected to both lower the heme midpoint potential and have significant effects on the induced CD (*33*, *50*) of the hemes, neither of which correlates with each other in the maquettes studied, suggesting that this is not the active mechanism. The relative equivalence of apo state helix content and the wide variation in global peptide stability indicate that changes in peptide secondary structure content and stability are not the sole causes of the change in E_m. In electrostatic terms, the pH dependence of the E_m value of $[I_6F_{13}A_{24}]_2$ is virtually identical to $[L_6L_{13}A_{24}]_2$, indicating that changes in the pK_a values of acid/base amino acid side chains involved in charge compensation are not effected by these hydrophobic core alterations. A most likely source of this effect is the extent to which the solvent exposure of the heme varies between these maquette scaffolds. Recent work

by Tezcan et al. on *c*-type cytochromes demonstrates that the 50 mV drop in potential may be accounted for by exposure of only an additional 4 Å^2 of porphyrin surface area (*51*). Significantly, the lowering of the E_m values in the sequence space variants parallels the gain in conformational specificity of the apopeptides. This result suggests that tighter protein−protein interactions in the apo state may result in incomplete sequestration of the first heme into the hydrophobic core and further access of water to the heme raising the local dielectric and, hence, lowering the reduction midpoint potential.

The presence of heme−heme charge interactions of >70 mV indicates the syn global topology of the diheme peptides and demonstrates cofactor−cofactor interactions within the hydrophobic cores of $[L_6L_{13}F_{24}]_2$ and each of the $[I_6F_{13}X_{24}]_2$ (X = A, I, F) maquettes (*52*). The magnitude of the interactions in the syn maquettes (72−132 mV) with a modeled Fe-to-Fe distance of ≈13 Å is slightly larger than the 62−77 mV heme−heme interaction observed in the tetraheme cytochrome subunit of the *Rhodopseudomonas viridis* reaction center with Fe-to-Fe distances of 14−16 Å (*53*). Additionally, the maquette ΔE_m values are significantly smaller than the 162 mV observed for the split-Soret cytochrome from *Desulfovibrio desulfuricans* ACC 27774, which has a shorter Fe-to-Fe distance of 9 Å (*54*). While the maquette scaffold is clearly capable of supporting local electrostatic fields in a dielectric medium similar to a natural multiheme cytochrome, the ΔE_m may not be solely attributable to heme−heme electrostatic interactions as has been suggested for the heme A−heme A_3 interaction in cytochrome *c* oxidase (*55*, *56*). The lowering of the second heme reduction potential may reflect greater solvent exposure of the second heme increasing the apparent ΔE_m.

Single amino acid changes per helix can alter the global topology of the two protein subunits as illustrated by the sequence space pathway peptides. In the diheme state where the global topology can be determined by electrochemistry, $[L_6L_{13}F_{24}]_2$ exists in a syn global topology, whereas $[I_6L_{13}F_{24}]_2$ and $[L_6F_{13}F_{24}]_2$ have an anti global topology and their combination, $[I_6F_{13}F_{24}]_2$, is syn. The alteration of the global topology either by single amino acid changes per helix or by cofactor incorporation has precedent in maquettes. The first generation prototype $[L_6L_{13}A_{24}]_2$ converts from a syn to anti global topology when a serine is placed at position 24, $[L_6L_{13}S_{24}]_2$ (*38*), or when two bound hemes B (syn) are replaced with two hemes A (anti) (*9*). Additionally, bulky flavins covalently linked to interior cysteine residues alter the syn−anti equilibrium in a helix−loop−helix maquette scaffold (*8*). Since the energetic differences between syn and anti may be relatively small in maquettes compared to the measured global stabilities (>18 kcal/mol), the iterative protein redesign strategy we have developed to transform multistructured peptides into proteins with singular structure relies on some degree of backbone and side chain freedom, a feature uncommon to many structure-based redesign algorithms (*57*−*61*).

When the stepwise sequence modifications are viewed in sequence space, there are hints that successful results obtained in one maquette scaffold may be transferable to related maquette. Thus, primary structure and perhaps function may be transferable between maquette scaffolds. First, the alanine to phenylalanine modifications at positions 24 in both $[I_6F_{13}A_{24}]_2$ and $[L_6L_{13}A_{24}]_2$ resulting in $[I_6F_{13}F_{24}]_2$ and $[L_6L_{13}F_{24}]_2$, respectively, show increased global conformational specificity due to local hydrophobic packing contacts. Second, the sequence space pathway detailed in this paper shown as follows:

$$[L_6L_{13}A_{24}]_2 \rightarrow [L_6L_{13}F_{24}]_2$$
(multistructured) (approaching a singular structure)

$$\rightarrow$$

$$[I_6L_{13}F_{24}]_2 \text{ or } [L_6F_{13}F_{24}]_2 \rightarrow [I_6F_{13}F_{24}]_2$$
(both single structured) (uniquely structured)

mimics the results found for the prototype, as follows:

$$[L_6L_{13}H_{24}]_2 \rightarrow$$
(multistructured)

$$[I_6L_{13}H_{24}]_2 \text{ or } [L_6F_{13}H_{24}]_2 \rightarrow$$
(two dominant structures) or (uniquely structured)

$$[I_6F_{13}H_{24}]_2$$
(uniquely structured)

indicating that hydrophobic packing arrangements derived from one maquette scaffold may be transferable to other scaffolds (*3*). Last, the retention of the E_m dependence on pH between $[L_6L_{13}A_{24}]_2$ and $[I_6F_{13}A_{24}]_2$ illustrates that functional properties may be transferable between related maquette scaffolds. If this concept of information transfer between maquette scaffolds holds up in continued studies, it will effectively multiply the results of any one maquette study by the number of maquette scaffolds.

Following the sequence space pathway between $[L_6L_{13}A_{24}]_2$ and $[I_6F_{13}F_{24}]_2$ reveals the precise amino acid changes responsible for altering the protein conformational specificity as well as the heme affinity and reduction potential as well as the effects of their combinations. This methodology provides more detailed insight into the role of second sphere amino acids (*62*, *63*) in controlling the properties of designed heme proteins than the results of combinatorial heme protein libraries (*41*, *64*, *65*) perhaps allowing for future rational design of heme properties (*66*). The results of fundamental studies of the consequences of steps in sequence space such as those described in this report may be effectively magnified by information transfer between maquette scaffolds as it may allow for their direct implementation in related scaffolds with predictable outcomes. Thus, the protein and cofactor binding site design rules delineated from one maquette may be transferable to novel scaffolds with predicable results increasing the efficiency of our hierarchical approach to heme protein design. As such, studies investigating feasibility of direct information transfer in maquettes are underway.

REFERENCES

1. Robertson, D. E., Farid, R. S., Moser, C. C., Urbauer, J. L., Mulholland, S. E., Pidikiti, R., Lear, J. D., Wand, A. J., DeGrado, W. F., and Dutton, P. L. (1994) *Nature 368*, 425−432.
2. Gibney, B. R., Rabanal, F., Skalicky, J. J., Wand, A. J., and Dutton, P. L. (1997) *J. Am. Chem. Soc. 119*, 2323−2324.
3. Gibney, B. R., Rabanal, F., Skalicky, J. J., Wand, A. J., and Dutton, P. L. (1999) *J. Am. Chem. Soc. 121*, 4952−4960.
4. Sharp, R. E., Diers, J. W., Bocian, D. F., and Dutton, P. L. (1998) *J. Am. Chem. Soc. 120*, 7103−7104.

5. Rabanal, F., DeGrado, W. F., and Dutton, P. L. (1996) *J. Am. Chem. Soc. 118*, 473−474.
6. Gibney, B. R., Johansson, J. S., Rabanal, F., Skalicky, J. J., Wand, A. J., and Dutton, P. L. (1997) *Biochemistry 36*, 2798−2806.
7. Gibney, B. R., Mulholland, S. E., Rabanal, F., and Dutton, P. L. (1996) *Proc. Natl. Acad. Sci. U.S.A. 93*, 15041−15046.
8. Sharp, R. E., Rabanal, F., Moser, C. C., and Dutton, P. L. (1998) *Proc. Natl. Acad. Sci. U.S.A. 95*, 10465−10470.
9. Gibney, B. R., Isogai, Y., Rabanal, F., Reddy, K. S., Grosset, A. M., Moser, C. C., and Dutton, P. L. (2000) *Biochemistry 39*, 11041−11049.
10. Gibney, B. R., Rabanal, F., Reddy, K. S., and Dutton, P. L. (1998) *Biochemistry 37*, 4635−4643.
11. Gibney, B. R., and Dutton, P. L. (1999) *Protein Sci. 8*, 1888−1898.
12. Xia, D., Yu, C.-A., Kim, H., Xia, J.-Z., Kachurin, A. M., Zhang, L., Yu, L., and Deisenhofer, J. (1997) *Science 277*, 60−66.
13. Zhang, Z., Huang, L., Shulmeister, V. M., Chi, Y.-I., Kim, K. K., Hung, L.-W., Crofts, A. R., Berry, E. A., and Kim, S.-H. (1998) *Nature 392*, 677−684.
14. Ding, H., Moser, C. C., Robertson, D. E., Tokito, M. K., Daldal, F., and Dutton, P. L. (1995) *Biochemistry 34*, 15979.
15. Bryson, J. W., Betz, S. F., Lu, H. S., Suich, D. J., Zhou, H. X., O'Neil, K. T., and DeGrado, W. F. (1995) *Science 270*, 935−941.
16. Johansson, J. S., Gibney, B. R., Skalicky, J. J., Wand, A. J., and Dutton, P. L. (1998) *J. Am. Chem. Soc. 120*, 3881−3886.
17. Mulholland, S. E., Gibney, B. R., Rabanal, F., and Dutton, P. L. (1998) *J. Am. Chem. Soc. 120*, 10296−10302.
18. Grosset, A. M., Rabanal, F., Farid, R. S., Roberston, D. E., DeGrado, W. F., and Dutton, P. L. (1996) *Peptides: Chemistry, Structure and Biology* (Kaumaya, T. P., and Hodges, R. S. Eds.) pp 573−574, Mayflower Scientific, Columbus, OH.
19. Shifman, J. M., Moser, C. C., Kalsbeck, W. A., Bocian, D. F., and Dutton, P. L. (1998) *Biochemistry 37*, 16815−16827.
20. Skalicky, J. J., Bieber, R. J., Gibney, B. R., Rabanal, F., Dutton, P. L., and Wand, A. J. (1998) *J. Biomol. NMR 11*, 227−228.
21. Skalicky, J. J., Gibney, B. R., Rabanal, F., Bieber-Urbauer, R. J., Dutton, P. L., and Wand, A. J. (1999) *J. Am. Chem. Soc. 121*, 4941−4951.
22. Bodanszky, M. (1993) *Peptide Chemistry: A Practical Approach*, 2nd ed., Springer-Verlag, New York.
23. Mok, Y.-K., De Prat Gay, G., Butler, P. J., and Bycroft, M. (1996) *Protein Sci. 6*, 310.
24. Price, N. C., and Dwek, R. A. (1979) *Principles and Problems in Physical Chemistry for Biochemists*, 2nd ed., Oxford Universtiy Press, Oxford.
25. Dutton, P. L. (1978) *Methods Enzymol. 54*, 411.
26. Gibney, B. R., Skalicky, J. J., Wand, A. J., and Dutton, P. L. (2001) *J. Am. Chem. Soc.* (submitted for publication).
27. Perutz, M. F. (1978) *Sci. Am. 239*, 92−125.
28. O'Neil, K. T., and DeGrado, W. L. (1990) *Science* 250, 646−651.
29. Pace, C. N. (1986) *Methods Enzymol. 131*, 266−280.
30. Rivera, M., Wells, M. A., and Walker, F. A. (1994) *Biochemistry 33*, 2161−2170.
31. Myer, Y. P., and Pande, A. (1978) in *The Porphyrins* (Dolphin, D., Ed.) Vol. III, pp 271−322, Academic Press, New York.
32. Nakanishi, K., Berova, N., and Woody, R. W., Eds. (1994) *Circular Dichroism Principles and Applications*, p 570, VCH Publishers, Inc., New York.
33. Blauer, G., Sreerama, N., and Woody, R. W. (1993) *Biochemistry 32*, 6674−6679.
34. Hsu, M. C., and Woody, R. W. (1971) *J. Am. Chem. Soc. 93*, 3515−3525.
35. Chance, B., Crofts, A. R., Mishimura, M., and Price, B. (1970) *Eur. J. Biochem. 13*, 364−374.
36. Louro, R. O., Catarino, T., LeGall, J., and Xavier, A. V. (1997) *J. Biol. Inorg. Chem. 2*, 488−491.
37. Chen, X., Disher, B. M., Pilloud, D. L., Moser, C. C., Gibney, B. R., and Dutton, P. L. (2001) *J. Phys. Chem. B* (manuscript in preparation).
38. Grosset, A. M., Gibney, B. R., Rabanal, F., Moser, C. C., and Dutton, P. L. (2001) *Biochemistry 40*, 5474−5487.
39. Kalsbeck, W. A., Roberston, D. E., Pandey, R. K., Smith, K. M., Dutton, P. L., and Bocian, D. F. (1996) *Biochemistry 35*, 3429−3238.
40. Feng, Y., Sligar, S. G., and Wand, A. J. (1994) *Nat. Struct. Biol. 1*, 30−35.
41. Cocco, M. J., Kao, Y. H., Phillips, A. T., and Lecomte, J. T. (1992) *Biochemistry 31*, 6481−6491.
42. Englander, S. W., Sosnick, T. R., Mayne, L. C., Shtilerman, M., Qi, P. X., and Bai, Y. (1998) *Acc. Chem. Res. 31*, 737−744.
43. Springs, S. L., Bass, S. E., and McLendon, G. L. (2000) *Biochemistry 39*, 6075−6082.
44. Kay, C. J., and Lippay, E. W. (1992) *Biochemistry 31*, 11376−11382.
45. Sarma, S., DiGate, R. J., Goodin, D. B., Miller, C. J., and Guiles, R. D. (1997) *Biochemistry 36*, 5658−5668.
46. Shelnutt, J. A., Song, X. Z., Ma, J. G., Jia, S. L., Jentzen, W., and Medforth, C. J. (1998) *Chem. Soc. Rev. 27*, 31−41.
47. Kennedy, M. L., Silchenko, S., Houndonougbo, N., Gibney, B. R., Dutton, P. L., Rodgers, K. R., and Benson, D. R. (2001) *J. Am. Chem. Soc. 123*, 4635−4636.
48. Gunner, M. R., Alexov, E., Torres, E., and Lipovaca, S. (1997) *J. Biol. Inorg. Chem. 2*, 126−134.
49. Stellwagen, E. (1978) *Nature 275*, 73−74.
50. Barkigia, K. M., Chantranupong, L., Smith, K. M., and Fajer, J. (1988) *J. Am. Chem. Soc. 110*, 7566−7567.
51. Tezcan, F. A., Winkler, J. R., and Gray, H. B. (1998) *J. Am. Chem. Soc. 120*, 13383−13388.
52. Shifman, J. M., Gibney, B. R., Sharp, R. E., and Dutton, P. L. (2000) *Biochemistry 39*, 14813−14821.
53. Gunner, M. R., and Honig, B. (1991) *Proc. Natl. Acad. Sci., U.S.A. 88*, 9151−9155.
54. Matias, P. M., Morias, J., Coelho, A. V., Meijers, R., Gonzales, A., Thompson, A. J., Sieker, L., LeGall, J., and Carrondo, M. A. (1997) *J. Biol. Inorg. Chem. 2*, 507−514.
55. Wikström, M. K. F., Harmon, H. J., Ingledew, W. J., and Chance, B. (1976) *FEBS Lett. 65*, 259−277.
56. Hosler, J. P., Fetter, J., Tecklenburg, M. M., Espe, M., Lerma, C., and Ferguson-Miller, S. (1992) *J. Biol. Chem. 267*, 24264−23272.
57. Dahiyat, B. I., and Mayo, S. L. (1997) *Science 278*, 82−87.
58. Desjarlais, J. M., and Handel, T. M. (1995) *Protein Sci. 4*, 2006−2018.
59. Jiang, X., Bishop, E. J., and Farid, R. S. (1997) *J. Am. Chem. Soc. 119*, 838−839.
60. Jiang, X., Farid, H., Pistor, E., and Farid, R. S. (2000) *Protein Sci. 9*, 415−428.
61. Hellinga, H. W. (1998) *Folding Des. 3*, R1−R8.
62. Karlin, S., Zhu, Z.-Y., and Karlin, K. D. (1997) *Proc. Natl. Acad. Sci. U.S.A. 94*, 14225−14230.
63. Karlin, S., and Zhu, Z.-Y. (1997) *Proc. Natl. Acad. Sci. U.S.A. 94*, 14231−14236.
64. Rojas, N. R. L., Kamtekar, S., Simons, C. T., Mclean, J. E., Vogel, K. M., Spiro, T. G., Farid, R. S., and Hecht, M. H. (1997) *Protein Sci. 6*, 2512−2524.
65. Rau, H. K., DeJonge, N., and Haehnel, W. (2000) *Angew. Chem., Int. Ed. 39*, 250−253.
66. Gibney, B. R., and Dutton, P. L. (2001) in *Advances in Inorganic Chemistry* (Mauk, A. G., and Sykes, A. G., Eds.) Vol. 51, pp 409−455, Academic Press, New York.

BI002806H